Added value of contrast enhancement boost images in routine multiphasic contrast-enhanced CT for the diagnosis of small (<20 mm) hypervascular hepatocellular carcinoma

Yabe, Shinji ; Sofue, Keitaro ; Hori, Masatoshi ; Maebayashi, Tomoki ; Nishigaki, Megumi ; Tsujita, Yushi ; Yamaguchi, Takeru ; Ueshima,…

(Citation)
European Journal of Radiology,160:110696

(Issue Date)
2023-03

(Resource Type)
journal article

(Version)
Version of Record

European Journal of Radiology 160 (2023) 110696

Contents lists available at ScienceDirect

European Journal of Radiology

journal homepage: www.elsevier.com/locate/ejrad

Added value of contrast enhancement boost images in routine multiphasic contrast-enhanced CT for the diagnosis of small (<20 mm) hypervascular hepatocellular carcinoma

Shinji Yabe [a], Keitaro Sofue [a], Masatoshi Hori [a,*], Tomoki Maebayashi [b], Megumi Nishigaki [c], Yushi Tsujita [a], Takeru Yamaguchi [a], Eisuke Ueshima [a], Yoshiko Ueno [a], Takamichi Murakami [a]

[a] Department of Radiology, Kobe University Graduate School of Medicine, 7-5-2 Kusunoki-cho, Chuo-ku, Kobe 650-0017, Japan
[b] Center for Radiology and Radiation Oncology, Kobe University Hospital, 7-5-2 Kusunoki-cho, Chuo-ku, Kobe 650-0017, Japan
[c] Canon Medical Systems Corporation, 1385 Shimoishigami, Otawara, Tochigi 324-8550, Japan

ARTICLE INFO

Keywords:
Hepatocellular carcinoma
CT
Subtraction technique
Diagnostic imaging

ABSTRACT

Purpose: To investigate the added value of contrast enhancement boost (CE-boost) images in multiphasic contrast-enhanced CT (CE-CT) for diagnosing small (<20 mm) hypervascular hepatocellular carcinoma (HCC).
Materials and methods: This retrospective study included 69 patients (age, 74 ± 8 years; 52 men) with 70 hypervascular HCCs (<20 mm) who underwent multiphasic CE-CT (pre-contrast, late arterial phase [LAP], portal venous phase [PVP], and equilibrium phase). Two types of CE-boost images were generated by subtracting PVP from LAP (LA-PV) images and LAP from PVP (PV-LA) images to enhance the contrast effect of hepatic arterial and portal venous perfusion more selectively. Tumor-to-liver contrast-to-noise ratios (CNRs) in CE-boost images were compared with those in CE-CT images using the Wilcoxon signed-rank test. Two independent readers reviewed the imaging datasets: CE-CT alone and CE-CT with CE-boost images. The diagnostic performance of each dataset was compared using jackknife alternative free-response receiver operating characteristics (JAFROC-1).
Results: The tumor-to-liver CNRs in the LA-PV (6.4 ± 3.0) and PV-LA (−3.3 ± 2.1) images were greater than those in the LAP (3.2 ± 1.7) and PVP images (−1.1 ± 1.4) (p <.001 for both). The reader-averaged figures of merit were 0.751 for CE-CT alone and 0.807 for CE-CT with CE-boost images (p <.001). Sensitivities increased by adding CE-boost images for both readers (p <.001 and = 0.03), while positive predictive values were equivalent (p >.99).
Conclusion: Adding CE-boost images to multiphasic CE-CT can improve the diagnostic accuracy and sensitivity for small hypervascular HCC by increasing the tumor-to-liver CNR.

1. Introduction

Multiphasic contrast-enhanced CT (CE-CT) plays an important role in hepatocellular carcinoma (HCC) diagnosis. A combination of arterial phase hyperenhancement and delayed washout is a radiological hallmark of HCC, and pathological confirmation is not always necessary prior to treatment [1,2]. Multiphasic CE-CT is commonly used to evaluate HCC because of its availability and high spatial resolution [3,4]. However, for detecting small (<20 mm in diameter) HCCs, accurate diagnosis using CE-CT is challenging because of its low sensitivity [4–6]. Arterial phase hyperenhancement and delayed washout are sometimes indistinct in small lesions [7,8], and improving tumor-to-liver contrast in CE-CT is desirable for detecting small HCCs. Several attempts, including low-tube-voltage CT and dual-energy CT, have been made to improve the tumor-to-liver contrast, especially to improve the detectability and conspicuity of arterial phase hyperenhancement [9–16]. Although a combination of CT hepatic arteriography and CT during arterial portography is a solution to address this problem and previous

Abbreviations: HCC, hepatocellular carcinoma; CE-CT, contrast-enhanced computed tomography; CE-boost, contrast enhancement boost; LAP, late arterial phase; PVP, portal venous phase; JAFROC, jackknife alternative free-response operating characteristic; FOM, figure of merit; CNR, contrast-to-noise ratio; LA-PV, PVP subtracted from LAP; PV-LA, LAP subtracted from PVP.

* Corresponding author.
E-mail address: horimsts@med.kobe-u.ac.jp (M. Hori).

https://doi.org/10.1016/j.ejrad.2023.110696
Received 4 October 2022; Received in revised form 30 December 2022; Accepted 10 January 2023
Available online 12 January 2023

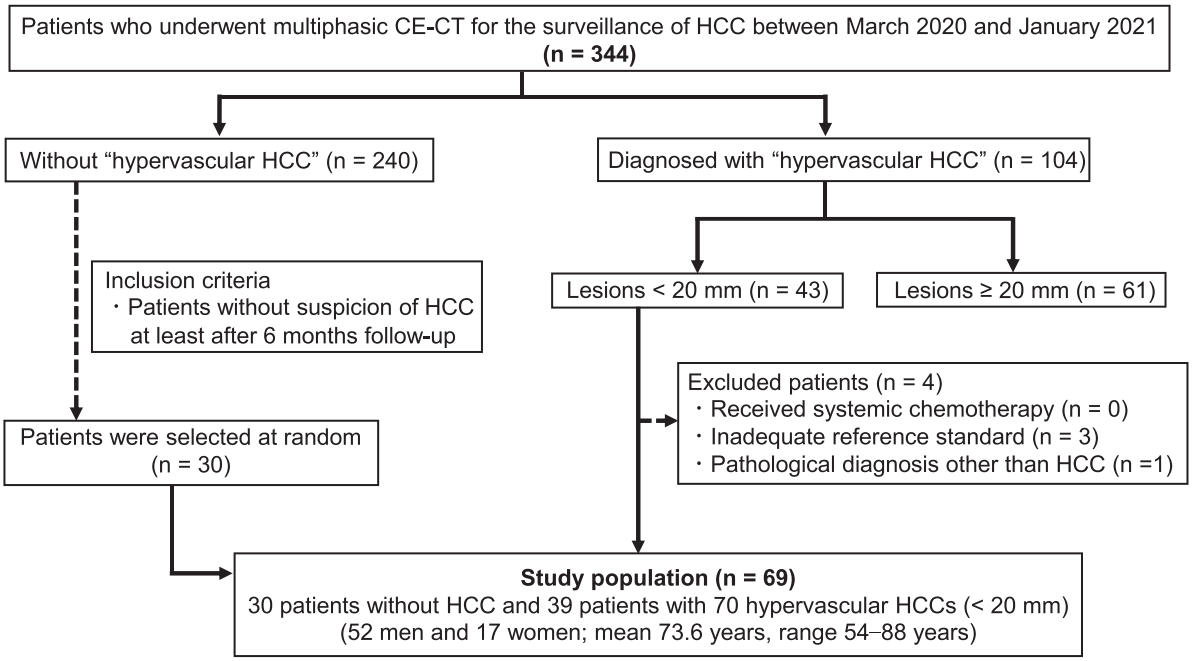

Fig. 1. Flowchart of the patient enrolment process. CE-CT, contrast-enhanced CT; HCC, hepatocellular carcinoma.

studies have shown better sensitivity [17,18], it is unsuitable for HCC surveillance due to its invasiveness [19].

Recently, the contrast enhancement boost (CE-boost; Canon Medical Systems, Otawara, Japan) technique has been proposed to increase the degree of contrast enhancement. In this technique, a subtraction image is obtained using a new subtraction algorithm (SURE subtraction iodine mapping, Canon Medical Systems) [20] and added to the original image with a denoising procedure. When a CE-boost image is created by subtracting the non-contrast images from the contrast phase images, the degree of the contrast effect can be increased [21]. This may improve the diagnostic performance for HCC detection. However, we believe that the CE-boost technique could generate new types of images instead of simply increasing the degree of contrast enhancement on multiphasic CE-CT. Because of the dual blood supply to the liver, the late arterial phase (LAP) and portal venous phase (PVP) images in CE-CT contain mixed hepatic arterial and portal venous perfusion in different proportions [22–24]. Accordingly, we devised and generated two types of CE-boost images by subtracting PVP from LAP (LA-PV) images and LAP from PVP (PV-LA) images, which showed less overlap between arterial and portal venous contrast enhancement. The purpose of this study was to investigate the added value of CE-boost images in multiphasic CE-CT for diagnosing small (<20 mm in diameter) hypervascular HCC.

2. Materials and Methods

2.1. Study population

This retrospective study was approved by the institutional review board, and the requirement for written informed consent was waived. Between March 2020 and January 2021, 344 consecutive patients with chronic liver disease underwent multiphasic CE-CT for HCC surveillance (Fig. 1). A board-certified radiologist (S.Y. with 2 years of experience in abdominal imaging) who had not participated in the qualitative analysis reviewed the multiphasic CE-CT images in reference to any available clinical information, serial follow-up images, and other imaging examinations. The inclusion criteria were *(a)* patients who had hypervascular HCC, and *(b)* largest lesion diameter < 20 mm. The exclusion criteria were *(a)* patients who received systemic chemotherapy, *(b)* inadequate reference standard (see Lesion Confirmation section below for details), and *(c)* pathological diagnosis other than HCC.

A group of patients without HCC was also selected. The inclusion criteria were *(a)* patients who did not have hypervascular HCC on the initial multiphasic CE-CT, and *(b)* patients in whom follow-up imaging examinations performed more than 6 months later showed no suspicious findings for HCC. From these, 30 patients were selected using a random number table.

2.2. Lesion Confirmation: Standard of reference

Thirty-nine of the 69 enrolled patients had 70 confirmed hypervascular hepatocellular carcinomas (HCCs). An abdominal radiologist (S.Y.) confirmed the presence of hypervascular HCCs. Pathological proof of focal lesions was obtained after surgery in 13 patients (15 nodules). In 19 patients (39 nodules), typical angiographic findings and sustained iodized oil accumulation after transcatheter chemoembolization therapy, confirmed by serial follow-up CT, were used to diagnose HCC. For the other seven patients (16 nodules), HCCs were diagnosed using the Liver Imaging Reporting and Data System [25]. For lesions 10–19 mm (13 nodules), LR-5 on multiphasic contrast-enhanced CT or serial follow-up images were used to diagnose HCC. For lesions < 10 mm (three nodules), lesions that grew to more than 10 mm and showed LR-5 on follow-up images were regarded as HCC. The mean follow-up period was 12.2 ± 4.7 months.

2.3. CT technique

Multiphasic CE-CT images were obtained using a 320-row CT scanner (Aquilion ONE GENESIS Edition; Canon Medical Systems). The multiphasic protocol was composed of pre-contrast, LAP, PVP, and equilibrium phases. Further information can be found in Supplementary Methods.

2.4. Post-Processing and image reconstruction

Two types of CE-boost images were derived using an advanced image subtraction technique (SURE subtraction iodine mapping). The technique was implemented using non-rigid registration and image subtraction (Fig. 2). CE-boost (LA-PV) images were generated by

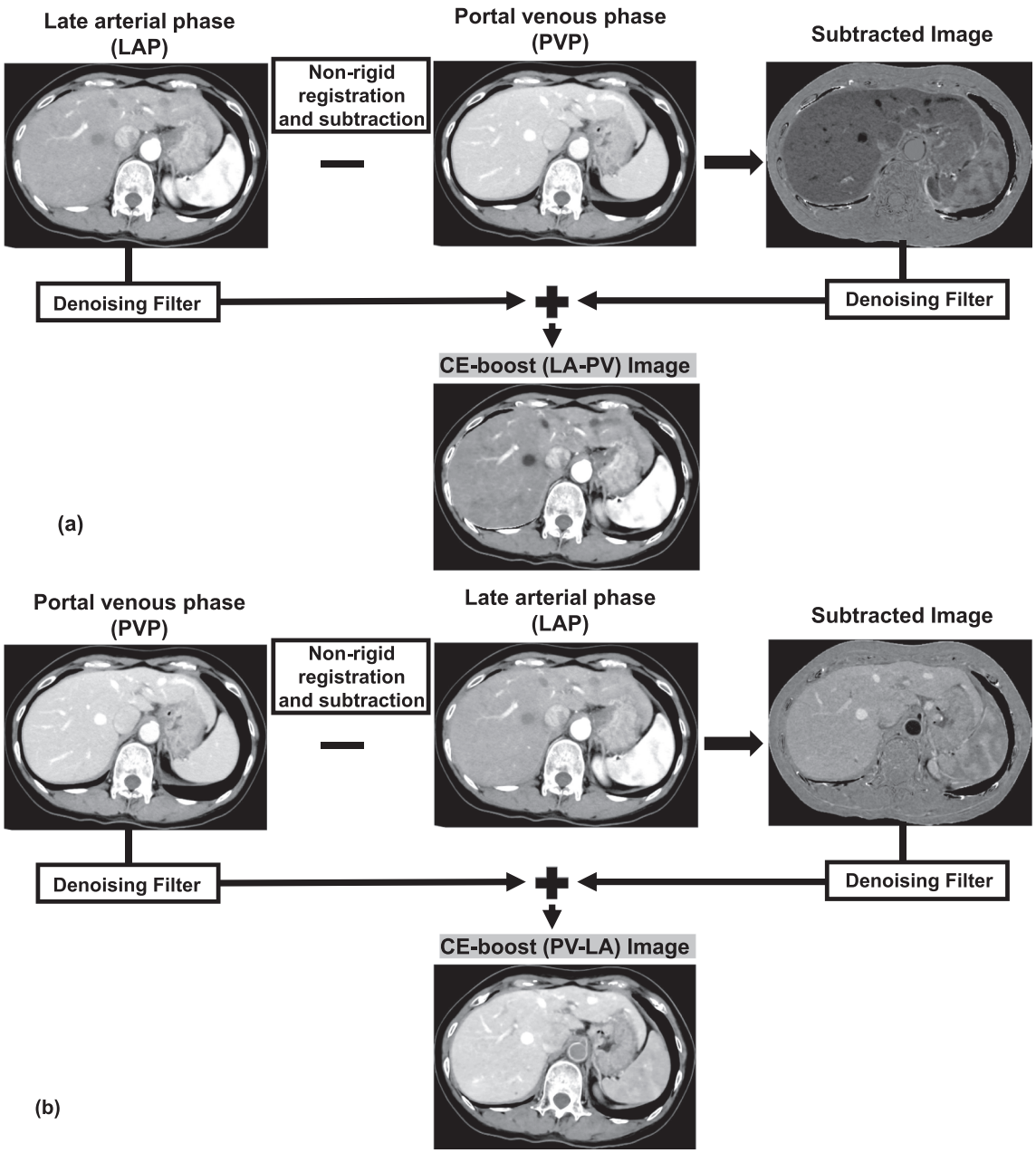

Fig. 2. Schema of CE-boost images. In the CE-boost (LA-PV) image **(a)**, the subtracted image is derived by subtracting the PVP image from the LAP image. Then, the LAP and subtracted images are fused after a denoising process; thus, contrast enhancement in LAP is emphasized, whereas contrast enhancement in PVP is suppressed. In the CE-boost (PV-LA) image **(b)**, the subtracted image is derived by subtracting the LAP image from the PVP image. Then, the PVP and subtracted images are fused after a denoising process; thus, contrast enhancement in PVP is emphasized, whereas contrast enhancement in LAP is suppressed. CE-boost, contrast enhancement boost; LA-PV, PVP subtracted from LAP; PV-LA, LAP subtracted from PVP; PVP, portal venous phase; LAP, late arterial phase.

subtracting PVP from LAP images, and CE-boost (PV-LA) images were generated by subtracting LAP from PVP images. In CE-boost (LA-PV) images, hepatic arterial perfusion is emphasized (Fig. 2a). Likewise, portal venous perfusion was emphasized in CE-boost (PV-LA) images (Fig. 2b).

Conventional multiphasic CE-CT images for LAP and PVP were reconstructed in 0.5-mm slices at 0.5-mm intervals. CE-boost (LA-PV) and (PV-LA) images were generated from the thin-slice image data. CE-CT and CE-boost thin-slice images were used for quantitative image analysis. For qualitative image analysis, CE-CT and CE-boost images were reconstructed in 5-mm slices at 5-mm intervals.

2.5. Quantitative image analysis

Quantitative measurements were performed by an abdominal radiologist (S.Y.) using a commercially available workstation (Ziostation 2 Type1000; Ziosoft, Newark, CA). CE-CT (LAP and PVP) images and the corresponding CE-boost (LA-PV and PV-LA) images were displayed simultaneously for each patient.

The CT numbers (in Hounsfield units) of the liver parenchyma and hypervascular HCCs were obtained by manually placing circular regions of interest. Image noise was measured as the standard deviation of the ovoid region of interest drawn in the subcutaneous fat of the anterior wall. Details of the measurements are described in Supplementary Methods.

The tumor-to-liver contrast-to-noise ratio (CNR) was calculated

using the following formula: $CNR = (ROI_{lesion} - ROI_{liver}) / SD_{noise}$, where ROI_{lesion} is the attenuation of hypervascular HCCs, ROI_{liver} is the mean attenuation of the liver parenchyma, and SD_{noise} represents the standard deviation of the subcutaneous fat. For all measurements, the size, shape, and position of the regions of interest were kept constant by applying a multidata fusion function of the workstation.

2.6. Qualitative image analysis

The images were anonymized and transferred to an image viewer (EV Insite S; PSP Corporation). Two abdominal radiologists (M.H. and K. S. with 25 and 15 years of experience in abdominal imaging, respectively) separately and independently reviewed two imaging data sets of all 69 patients in random order for the diagnosis of hypervascular HCCs: multiphasic CE-CT alone and multiphasic CE-CT with CE-boost images. The readers were aware that the patients might have hypervascular HCCs but were blinded to any clinical information and the patient proportions in the two groups. First, the readers evaluated only multiphasic CE-CT images, including pre-contrast, LAP, PVP, and equilibrium phase images in the first reading session. They recorded the presence and location of the lesions using the following four-point confidence scale: 1, probably not HCC; 2, possibly HCC; 3, probably HCC; and 4, definitely HCC. Details of confidence scale evaluation are described in the Supplementary Methods. Immediately after the first reading session, two types of CE-boost (LA-PV and PV-LA) images were presented to the readers along with multiphasic CE-CT images. The readers referred to the multiphasic CE-CT and CE-boost images and recorded changes in lesion presence, location, and confidence rating. In evaluating the dataset of multiphasic CE-CT with CE-boost images, the CE-boost images were used mainly for lesion detection; then, the confidence scores were determined comprehensively using both multiphasic CE-CT and CE-boost images.

The readers were also asked to rate the misregistration of CE-boost images focusing on the contour of the liver using the following four-point scale: 1, severe misregistration; 2, moderate misregistration; 3, slight misregistration; and 4, almost no misregistration. Disagreements between the two readers were resolved by a consensus review after the reading session.

Additionally, the abdominal radiologist (S.Y.), who performed the quantitative image analysis, reviewed all CE-boost images to determine if characteristic artifacts near the liver cysts were present and evaluated if the artifacts affected the diagnostic performance of the technique for each patient. The characteristic artifacts observed only on the CE-boost images were noticed by an abdominal radiologist during a preliminary review of the images. Therefore, we investigated the occurrence frequency of artifacts and evaluated their effects on image interpretation.

2.7. Statistical analysis

Continuous variables were summarized as mean ± standard deviation, whereas categorical variables were presented as counts and frequencies. Wilcoxon signed-rank tests were used to compare the liver and lesion attenuation, image noise, and tumor-to-liver CNR between the CE-CT (LAP and PVP) images and the corresponding CE-boost (LA-PV and PV-LA) images.

The performance of the two imaging datasets for detecting hypervascular HCCs was evaluated and compared using jackknife alternative free-response receiver operating characteristic (JAFROC-1) analysis (JAFROC version 4.2.1; https://github.com/dpc10ster/WindowsJafroc) [26]. Mean diagnostic accuracy was estimated according to the mean figure of merit (FOM) from the area under the JAFROC curve [27]. Regarding the confidence scale used to detect hypervascular HCCs, the inter-reader agreement was evaluated using unweighted kappa statistics. Sensitivity and positive predictive values per lesion and sensitivity, specificity, accuracy, and positive and negative predictive values per patient were also compared using the McNemar test and Fisher's exact probability test. A confidence scale of 3 or 4 indicated a positive diagnosis of HCC.

For all statistical analyses other than the JAFROC analysis, SPSS version 27.0 (IBM Corporation, Armonk, NY) was used. A p-value < 0.05 was considered to indicate a significant difference.

Table 1
Characteristics of 69 patients; 39 patients with 70 hypervascular hepatocellular carcinomas and 30 patients without hepatocellular carcinoma.

Characteristic	Total (n = 69)	Patients with HCC (n = 39)	Patients without HCC (n = 30)
Age (years) *	73.6 ± 8.3 (54–88)	74.7 ± 8.5 (54–88)	72.1 ± 7.8 (55–87)
Sex			
Male	52 (75.4)	24 (61.5)	28 (93.3)
Female	17 (24.6)	15 (38.5)	2 (6.7)
Height (cm) *	161.8 ± 8.9 (137–177)	159.0 ± 9.1 (137–173)	165.4 ± 7.1 (146–177)
Body weight (kg) *	61.7 ± 10.6 (41–85)	61.7 ± 11.2 (41–85)	61.8 ± 10.0 (45–84)
Treatment history			
Surgery	40 (58.0)	12 (30.8)	28 (93.3)
TACE	25 (36.2)	20 (51.3)	5 (16.7)
RFA	6 (8.7)	6 (15.4)	0 (0)
RT	3 (4.3)	1 (2.6)	2 (6.7)
None	10 (14.5)	10 (25.6)	0 (0)
Cause of liver disease			
HBV related	19 (27.5)	12 (30.8)	7 (23.3)
HCV related	29 (42.0)	19 (48.7)	10 (33.3)
Alcoholic	12 (17.4)	6 (15.4)	6 (20)
Other	9 (13.0)	2 (5.1)	7 (23.3)
Number of HCCs per patient			
0	30 (43.5)	…	30 (100)
1	22 (31.9)	22 (56.4)	…
2	11 (15.9)	11 (28.2)	…
3	1 (1.4)	1 (2.6)	…
4	4 (5.8)	4 (10.3)	…
7	1 (1.4)	1 (2.6)	…
Tumor size (mm) *	12.0 ± 4.1 (5–19)	12.0 ± 4.1 (5–19)	…
Number of HCCs (lesions)			
<10 mm	20 (28.6)	20 (28.6)	…
≥10 mm But < 20 mm	50 (71.4)	50 (71.4)	…

Unless otherwise specified, data are numbers of patients, with percentages in parentheses. * Data are means ± standard deviations, with ranges in parentheses. There are overlaps in treatment history, and total exceeds 100%. TACE, transcatheter arterial chemoembolization; RFA, radiofrequency ablation; RT, radiation therapy; HBV, hepatitis B virus; HCV, hepatitis C virus; HCC, hepatocellular carcinoma.

3. Results

A flowchart of the patient enrolment process is presented in Fig. 1. Thirty-nine patients with 70 small hypervascular HCCs (<20 mm diameter) and 30 patients without HCCs were included in this study. Diagnosis of HCC was confirmed by pathological proof in 13 patients and by several kinds of findings in the other patients. Finally, the study population comprised 69 patients (52 men and 17 women; mean age, 74 ± 8 years; range, 54–88 years) (Table 1). In addition to hypervascular HCCs, six hemangiomas were identified in four patients.

3.1. Quantitative image analysis

The mean number of hypervascular HCCs per patient was 1.8 (range, 1–7), with a mean size of 12.0 ± 4.1 mm (range, 5–19 mm). The mean image noises were lower on the LA-PV images (8.9 ± 1.6 HU) and PV-LA images (9.4 ± 1.7 HU) compared with the LAP (11.8 ± 1.2 HU) and PVP images (12.0 ± 1.3 HU) (p <.001 for both). The mean liver attenuations

Table 2
Liver and Tumor Attenuations, Image Noise Grades, and Tumor-to-Liver CNR.

	Late arterial phase			Portal venous phase		
	CE-CT	CE-boost (LA-PV)	*p* value	CE-CT	CE-boost (PV-LA)	*p* value
Liver attenuation (HU)	71.6 ± 10.6	51.0 ± 11.5	<0.001	111.9 ± 13.7	131.7 ± 16.3	<0.001
Tumor attenuation (HU)	107.5 ± 19.7	107.0 ± 24.6	0.45	96.2 ± 17.1	97.5 ± 16.9	0.16
Image noise (HU)	11.8 ± 1.2	8.9 ± 1.6	<0.001	12.0 ± 1.3	9.4 ± 1.7	<0.001
Tumor-to-liver CNR	3.2 ± 1.7	6.4 ± 3.0	<0.001	−1.1 ± 1.4	−3.3 ± 2.1	<0.001

Data are means ± standard deviations. CNR, contrast-to-noise ratio; CE-CT, contrast-enhanced CT; CE-boost, contrast enhancement boost; LA-PV, portal venous phase subtracted from late arterial phase; PV-LA, late arterial phase subtracted from portal venous phase; HU, Hounsfield unit.

were lower on the LA-PV images (51.0 ± 11.5 HU) than on the LAP images (71.6 ± 10.6 HU) and higher on the PV-LA images (131.7 ± 16.3 HU) than on the PVP images (111.9 ± 13.7 HU) (p <.001 for both). However, no significant differences were observed in the mean tumor attenuation between the CE-boost and CE-CT images. Thus, the tumor-to-liver CNRs in the LA-PV images (6.4 ± 3.0) and PV-LA images (-3.3 ± 2.1) were greater than those in the LAP (3.2 ± 1.7) and PVP images (-1.1 ± 1.4) (p <.001 for both) (Table 2, Fig. 3).

3.2. Diagnostic performance of each imaging data set for detecting hypervascular HCCs

The reader-averaged FOMs for detecting hypervascular HCCs were 0.751 (95% CI: 0.683, 0.818) for CE-CT alone and 0.807 (95% CI: 0.748, 0.866) for CE-CT with CE-boost images (Table 3). Between the two imaging data sets, the 95% CI for the difference in the FOM was −0.089 to −0.024, which was statistically significant for detecting hypervascular HCCs (F statistic = 12.04, p <.001). Inter-reader agreement for CE-CT alone and CE-CT with CE-boost images was moderate (kappa value = 0.49 for CE-CT alone and 0.41 for CE-CT with CE-boost images).

Adding CE-boost images improved per-lesion sensitivity from 40.0% (28/70) to 48.6% (34/70) for reader 1 (p =.03) and from 40.0% (28/70) to 57.1% (40/70) for reader 2 (p <.001) (Table 3, Figs. 4 and 5). The positive predictive values for both imaging data sets were high, with both readers performing above 95% without significant differences. With CE-CT alone, each reader made one false-positive diagnosis, which was confirmed as an arterioportal shunt on serial follow-up images; adding CE-boost images did not increase false-positive diagnoses. Although there were six hemangiomas, no lesions were misdiagnosed as HCC.

In a patient-based analysis, adding CE-boost images significantly improved the per-patient sensitivity and accuracy for reader 2, while there were no significant differences for reader 1 (Table 4). The per-patient specificity and positive and negative predictive values were not significantly different between the two imaging datasets for both readers.

3.3. Artifacts in CE-Boost images

Focusing on the contour of the liver, the degree of misregistration was rated 4 (almost no misregistration) in 100 (72.5%) images and 3 (slight misregistration) in 37 (26.8%) images. Only one image was rated 2 (moderate misregistration), but this was due to respiratory motion; the same finding was observed in the original CE-CT image. In 69 patients, no CE-boost images were rated 1 (severe misregistration).

Characteristic artifacts were identified near liver cysts in 10 patients (Fig. 6). These artifacts appeared as high attenuation areas on opposite sides of the liver cysts in both CE-boost (LA-PV and PV-LA) images in all

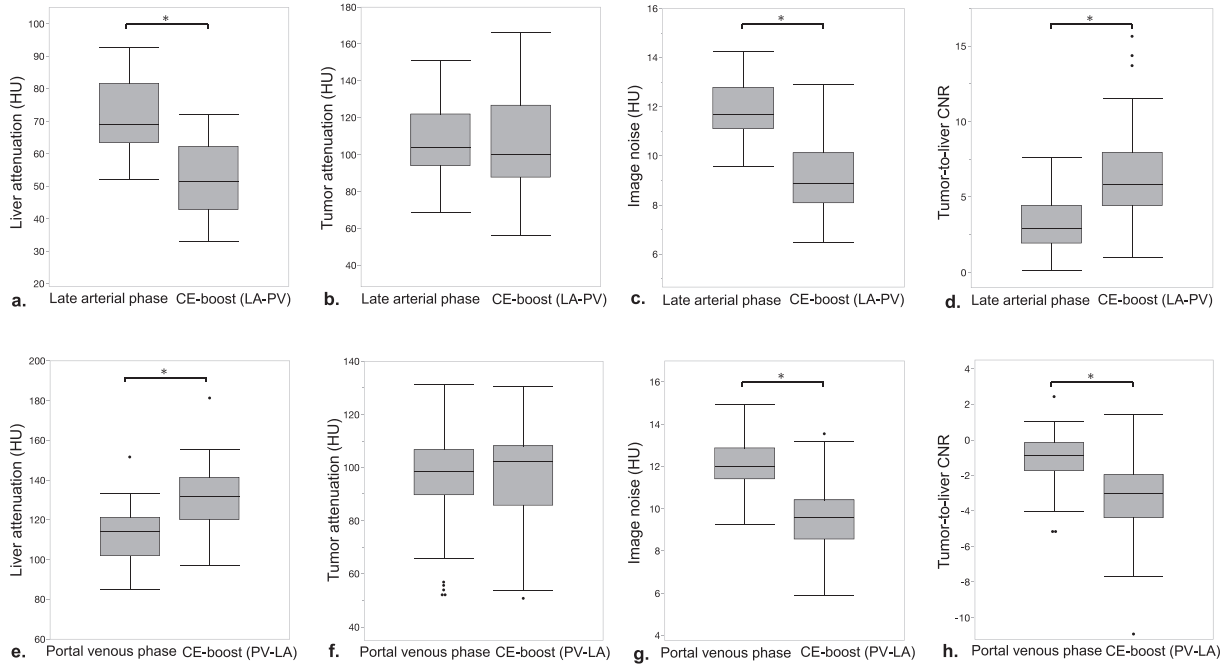

Fig. 3. Liver and tumor attenuations, image noise, and tumor-to-liver CNR. Box plots comparing the LAP images with the CE-boost (LA-PV) images **(a, b, c, d)** and the PVP images with the CE-boost (PV-LA) images **(e, f, g, h)**. The mean liver attenuation was different between the CE-CT and CE-boost images (p <.001 for both) **(a, e)**, whereas the mean tumor attenuation was not significantly different **(b, f)**. The mean image noises were significantly lower with the CE-boost images than with the CE-CT images (p <.001 for both) **(c, g)**. Tumor-to-liver CNRs in the CE-boost images were significantly greater than that of the CE-CT images (p <.001 for both) **(d, h)**. CNR, contrast-to-noise ratio; LAP, late arterial phase; CE-boost, contrast enhancement boost; LA-PV, PVP subtracted from LAP; PVP, portal venous phase; PV-LA, LAP subtracted from PVP; CE-CT, contrast-enhanced CT.

Table 3
Lesion-based diagnostic performance of multiphasic CE-CT alone and multiphasic CE-CT with CE-boost for small hypervascular hepatocellular carcinoma.

	CE-CT alone		CE-CT + CE-boost		
		95% CI		95% CI	*p* value
Reader 1					
FOM	0.725	0.647–0.804	0.765	0.685–0.844	0.047
Sensitivity (%)	40 (28/70)	28.5–52.4	48.6 (34/70)	36.4–60.8	0.03[a]
PPV (%)	96.6 (28/29)	82.2–99.9	97.1 (34/35)	85.1–99.9	1[b]
Reader 2					
FOM	0.776	0.698–0.854	0.860	0.796–0.924	0.006
Sensitivity (%)	40 (28/70)	28.5–52.4	57.1 (40/70)	44.8–68.9	0.0005[a]
PPV (%)	96.6 (28/29)	82.2–99.9	97.6 (40/41)	87.1–99.9	1[b]
Mean					
FOM	0.751	0.683–0.818	0.807	0.748–0.866	0.0009
Sensitivity (%)	40 (56/140)	31.8 – 48.6	52.9 (74/140)	44.2–61.3	<0.0001[a]
PPV (%)	96.6 (56/58)	88.1–99.6	97.4 (74/76)	90.8–99.7	1[b]

Numbers in parentheses are raw data. FOMs were estimated by using jackknife alternative free-response operating characteristic (JAFROC-1) software. [a] McNemar test. [b] Fisher's exact probability test. CE-CT, contrast-enhanced CT; CE-boost, contrast enhancement boost; CI, confidence interval; FOM, figure of merit; PPV, positive predictive value.

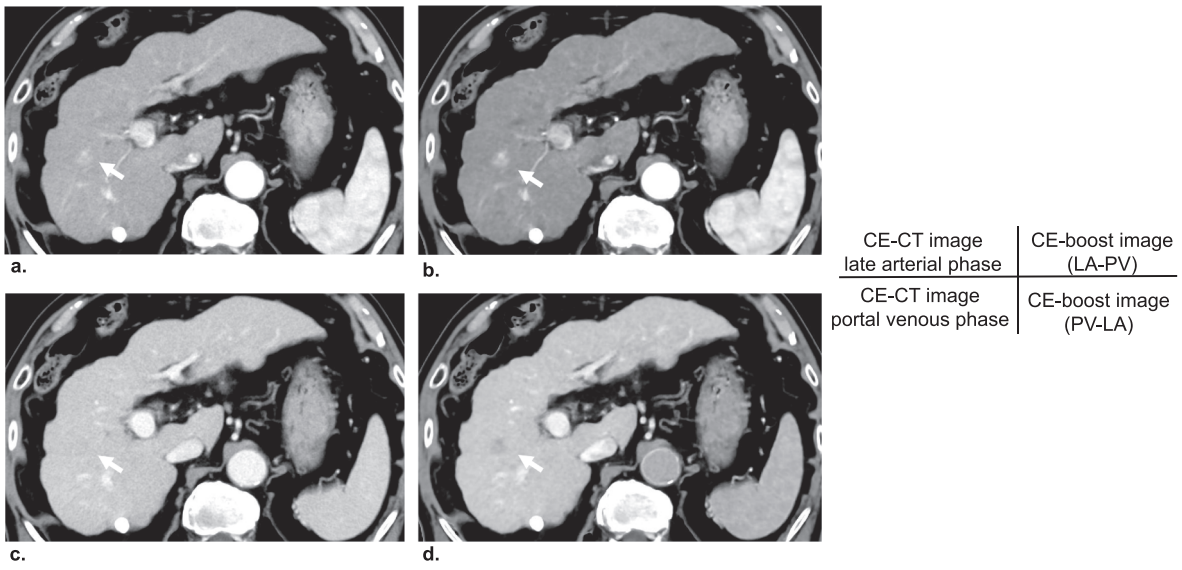

Fig. 4. HCC (arrow) in an 85-year-old man. **(a)** LAP image, **(b)** CE-boost (LA-PV) image, **(c)** PVP image, and **(d)** CE-boost (PV-LA) image. The lesion has faint arterial phase hyperenhancement without washout on the conventional CE-CT images **(a, c)**. The lesion shows nodular high attenuation on the CE-boost (LA-PV) image and low attenuation on the CE-boost (PV-LA) image **(b, d)**. Both readers rated the higher confidence for hypervascular HCC by adding the CE-boost images to the conventional CE-CT images. HCC, hepatocellular carcinoma; LAP, late arterial phase; CE-boost, contrast enhancement boost; LA-PV, PVP subtracted from LAP; PVP, portal venous phase; PV-LA, LAP subtracted from PVP; CE-CT, contrast-enhanced CT.

10 patients. Similar artifacts were not associated with HCC or hemangiomas. These artifacts were observed even when misregistration on the contour of the liver was not detected. These were not misdiagnosed as HCC, probably because the radiologists evaluated the images in conjunction with multiphasic CE-CT images.

4. Discussion

To increase the contrast effect of hepatic arterial and portal venous perfusion more selectively, we devised and generated two new types of images using the advanced image subtraction technique. CE-boost (LA-PV and PV-LA) images improved the tumor-to-liver CNRs compared with CE-CT (LAP and PVP) images. Moreover, adding CE-boost images to multiphasic CE-CT improved the diagnostic performance for detecting small (<20 mm) hypervascular HCC. Adding CE-boost images significantly improved per-lesion sensitivity for both readers, and there was no increase in false-positive diagnoses. We believe that the CE-boost images we devised will be useful for the management of patients with chronic liver disease that may develop into HCC.

A recent *meta*-analysis by Li et al. reported that sensitivity for small (<20 mm) HCC was 46% on CE-CT [6]. In our study, the sensitivity of multiphasic CE-CT alone was similarly low: 40% for both readers. To address this challenge of conventional CE-CT, we investigated the value of CE-boost (LA-PV and PV-LA) images, which effectively enhanced the contrast effect of the hepatic arterial and portal venous perfusion for the diagnosis of these small lesions. CE-boost (LA-PV) images improved the tumor-to-liver CNR 2.01 times compared with LAP images in hypervascular HCC. Low-tube-voltage and dual-energy CT reportedly improve the tumor-to-lesion CNR 1.35–2.06 times in LAP [10,13,15], similar to our study.

Compared with PVP images, CE-boost (PV-LA) images improved the tumor-to-liver CNR 2.97 times in our study. Reports on the improvement of delayed washout visualization using low-tube-voltage CT and dual-energy CT are limited. Matsuda et al. recently reported that 40 keV virtual monoenergetic images improved the tumor-to-liver CNR of HCC 1.48 times in the equilibrium phase [16], whereas our CE-boost (PV-LA) images showed superior results. Thus, CE-boost (LA-PV and PV-LA) imaging could effectively improve the tumor-to-liver CNR of

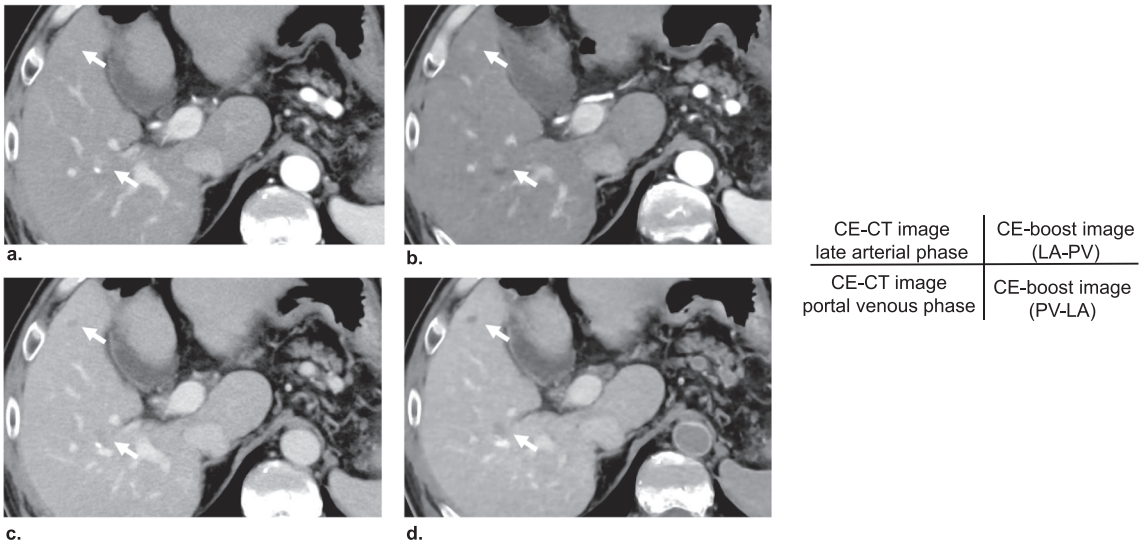

Fig. 5. HCCs (arrows) in a 57-year-old man. **(a)** LAP image, **(b)** CE-boost (LA-PV) image, **(c)** PVP image, and **(d)** CE-boost (PV-LA) image. Each lesion has faint arterial phase enhancement and washout on the conventional CE-CT images **(a, c)**. Corresponding CE-boost images demonstrate increased conspicuity of the lesions **(b, d)**. HCC, hepatocellular carcinoma; LAP, late arterial phase; CE-boost, contrast enhancement boost; LA-PV, PVP subtracted from LAP; PVP, portal venous phase; PV-LA, LAP subtracted from PVP; CE-CT, contrast-enhanced CT.

Table 4
Patient-based diagnostic performance of multiphasic CE-CT alone and multiphasic CE-CT with CE-boost for small hypervascular hepatocellular carcinoma.

	CE-CT alone		CE-CT + CE-boost		
		95% CI		95% CI	*p* value
Reader 1					
Sensitivity (%)	61.5 (24/39)	44.6–76.6	64.1 (25/39)	47.2–78.8	1[a]
Specificity (%)	96.7 (29/30)	82.8–99.9	96.7 (29/30)	82.8–99.9	1[a]
Accuracy (%)	76.8 (53/69)	65.1–86.1	78.3 (54/69)	66.7–87.3	1[a]
PPV (%)	96 (24/25)	79.6–99.9	96.2 (25/26)	80.4–99.9	1[b]
NPV (%)	65.9 (29/44)	50.1–79.5	67.4 (29/43)	51.5–80.9	1[b]
Reader 2					
Sensitivity (%)	64.1 (25/39)	47.2–78.8	87.2 (34/39)	72.6–95.7	0.004[a]
Specificity (%)	100 (30/30)	88.4–100	100 (30/30)	88.4–100	1[a]
Accuracy (%)	79.7 (55/69)	68.3–88.4	92.8 (64/69)	83.9–97.6	0.004[a]
PPV (%)	100 (25/25)	86.3–100	100 (34/34)	89.7–100	1[b]
NPV (%)	68.2 (30/44)	52.4–81.3	85.7 (30/35)	69.7–95.2	0.11[b]

Numbers in parentheses are raw data. [a] McNemar test. [b] Fisher's exact probability test. CE-CT, contrast-enhanced CT; CE-boost, contrast enhancement boost; CI, confidence interval; PPV, positive predictive value; NPV, negative predictive value.

hypervascular HCC. Consequently, we demonstrated that adding CE-boost images to multiphasic CE-CT images significantly improved the diagnostic performance for detecting small (<20 mm) hypervascular HCC, although the usefulness of low-tube-voltage CT and dual-energy CT for improving the diagnostic performance of small (<20 mm) HCC has not been demonstrated.

Severe misregistration in CE-boost images did not occur, whereas characteristic artifacts near liver cysts were observed in 10 patients. These artifacts were observed even when misregistration on the contour of the liver was not obvious, and they were most likely caused by misregistration of the cysts. Although we could not fully identify the cause of these artifacts, distortion caused by non-rigid registration potentially affected the subtraction image. These artifacts did not adversely affect diagnostic performance due to the evaluation in conjunction with multiphasic CE-CT images. Thus, a comprehensive evaluation of both CE-CT and CE-boost images is required for an accurate diagnosis.

As the CE-boost technique is based on a post-processing program, CE-boost images can be generated from routine clinical CE-CT imaging data without requiring raw data. The CE-boost technique does not require specialized hardware or specific image acquisition, which differs from low-tube-voltage or dual-energy CT. Additionally, it is advantageous to create images that emphasize hepatic arterial and portal venous perfusion more selectively, without invasiveness or increased radiation dose. Thus, the CE-boost technique is easier to apply in daily practice and can improve the diagnostic performance for small hypervascular HCC. Furthermore, CE-boost is technically feasible for use with low-tube-voltage CT or dual-energy CT, which may produce images with an even higher tumor-to-liver CNR, although further studies are needed.

This study has some limitations. First, due to the retrospective study design, selection bias may have occurred. Second, pathological proof was not obtained in some of the cases. However, we believe that the appropriate decision was made using several kinds of confirmatory findings as described in the lesion confirmation section. Third, CE-boost images have different characteristics of contrast effects than CE-CT images. Therefore, low attenuation on CE-boost (PV-LA) images does not mean "delayed washout," and an evaluation using only CE-boost images is not appropriate. Fourth, in the reading, only multiphase CE-CT images were evaluated first, followed by the addition of CE-boost images. The lack of separate reading may have affected the results of this study. However, considering the introduction of CE-boost images into clinical practice, we believe that the present method adequately simulates the actual clinical situation. Fifth, we did not measure added reading time by adding CE-boost images, and its effect on diagnostic performance is uncertain. Finally, although we included incidental benign lesions, such as arterioportal shunts and hemangiomas, no other types of liver lesions were included. The impact of the presence of other liver lesions on diagnostic performance is uncertain. In addition, we did not include hypovascular HCC in this study. The CE-boost technique may also be beneficial for the detection of hypovascular lesions. Therefore, further prospective studies with larger numbers of patients are warranted.

In conclusion, adding CE-boost images to multiphasic CE-CT can

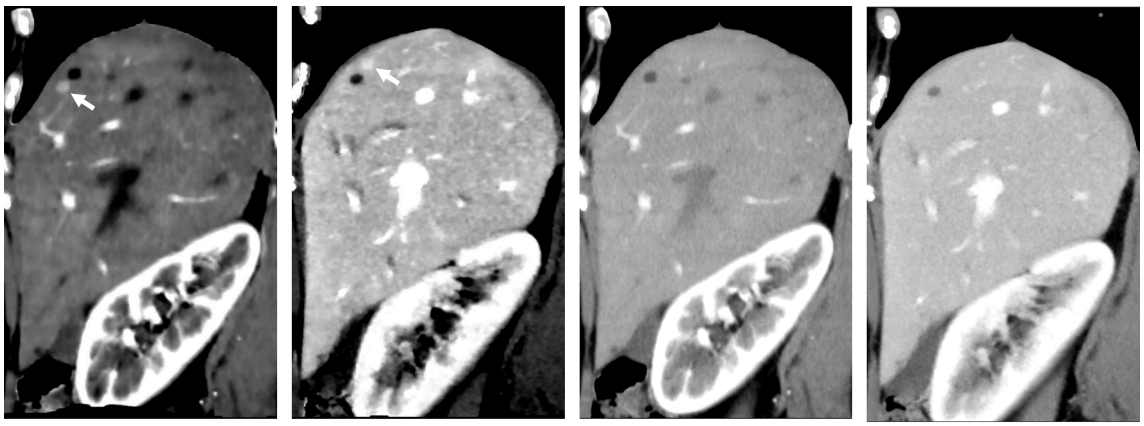

Fig. 6. Characteristic artifacts near cyst in CE-boost images. Sagittal images on **(a)** CE-boost (LA-PV), **(b)** CE-boost (PV-LA), **(c)** LAP, and **(d)** PVP images. A high attenuation area is seen adjacent to the edge of the liver cyst in the CE-boost (LA-PV) image **(arrow in a)**. A similar high attenuation area is depicted on the opposite side of the cyst in the CE-boost (PV-LA) image **(arrow in b)**. These artifacts are not observed in the multiphasic CE-CT images **(c, d)**. Although characteristic artifacts are seen, misregistration on the liver contour is not obvious **(a, b)**. Sagittal images are presented to better show the relative position of the cyst and the artifact. CE-boost, contrast enhancement boost; LA-PV, PVP subtracted from LAP; PV-LA, LAP subtracted from PVP; LAP, late arterial phase; PVP, portal venous phase; CE-CT, contrast-enhanced CT.

improve the diagnostic accuracy and sensitivity for small (<20 mm) hypervascular HCC by increasing the tumor-to-liver CNR. The CE-boost technique is potentially beneficial for the surveillance of small HCC.

Funding

This research did not receive any specific grant from funding agencies in the public, commercial, or not-for-profit sectors.

Declaration of Competing Interest

M.H. is supported by grants from Canon Medical Systems Corporation. M.N. is an employee of Canon Medical Systems Corporation.

Appendix A. Supplementary data

Supplementary data to this article can be found online at https://doi.org/10.1016/j.ejrad.2023.110696.

References

[1] J.A. Marrero, L.M. Kulik, C.B. Sirlin, A.X. Zhu, R.S. Finn, M.M. Abecassis, L.R. Roberts, J.K. Heimbach, Diagnosis, staging, and management of hepatocellular carcinoma: 2018 practice guidance by the American association for the study of liver diseases, Hepatology. 68 (2018) 723–750.

[2] A. Tang, M.R. Bashir, M.T. Corwin, I. Cruite, C.F. Dietrich, R.K.G. Do, E.C. Ehman, K.J. Fowler, H.K. Hussain, R.C. Jha, A.R. Karam, A. Mamidipalli, R.M. Marks, D. G. Mitchell, T.A. Morgan, M.A. Ohliger, A. Shah, K.-N. Vu, C.B. Sirlin, Evidence Supporting LI-RADS Major Features for CT- and MR Imaging–based Diagnosis of Hepatocellular Carcinoma: A Systematic Review, Radiology. 286 (2018) 29–48.

[3] S.H. Kim, D. Choi, S.H. Kim, J.H. Lim, W.J. Lee, M.J. Kim, H.K. Lim, S.J. Lee, Ferucarbotran-enhanced MRI versus triple-phase MDCT for the preoperative detection of hepatocellular carcinoma, AJR Am. J. Roentgenol. 184 (4) (2005) 1069–1076.

[4] M. Tsurusaki, K. Sofue, H. Isoda, M. Okada, K. Kitajima, T. Murakami, Comparison of gadoxetic acid-enhanced magnetic resonance imaging and contrast-enhanced computed tomography with histopathological examinations for the identification of hepatocellular carcinoma: a multicenter phase III study, J. Gastroenterol. 51 (2016) 71–79.

[5] R.F. Hanna, V.Z. Miloushev, A.n. Tang, L.A. Finklestone, S.Z. Brejt, R.S. Sandhu, C. S. Santillan, T. Wolfson, A. Gamst, C.B. Sirlin, Comparative 13-year meta-analysis of the sensitivity and positive predictive value of ultrasound, CT, and MRI for detecting hepatocellular carcinoma, Abdom Radiol (NY). 41 (1) (2016) 71–90.

[6] J. Li, J. Wang, L. Lei, G. Yuan, S. He, The diagnostic performance of gadoxetic acid disodium-enhanced magnetic resonance imaging and contrast-enhanced multi-detector computed tomography in detecting hepatocellular carcinoma: a meta-analysis of eight prospective studies, Eur. Radiol. 29 (2019) 6519–6528.

[7] M. Di Martino, D. Marin, A. Guerrisi, M. Baski, F. Galati, M. Rossi, S. Brozzetti, R. Masciangelo, R. Passariello, C. Catalano, Intraindividual Comparison of Gadoxetate Disodium–enhanced MR Imaging and 64-Section Multidetector CT in the Detection of Hepatocellular Carcinoma in Patients with Cirrhosis, Radiology. 256 (3) (2010) 806–816.

[8] U. Motosugi, T. Ichikawa, H. Sou, K. Sano, L. Tominaga, A. Muhi, T. Araki, Distinguishing hypervascular pseudolesions of the liver from hypervascular hepatocellular carcinomas with gadoxetic acid-enhanced MR imaging, Radiology. 256 (1) (2010) 151–158.

[9] D. Marin, R.C. Nelson, E. Samei, E.K. Paulson, L.M. Ho, D.T. Boll, D.M. DeLong, T. T. Yoshizumi, S.T. Schindera, Hypervascular liver tumors: low tube voltage, high tube current multidetector CT during late hepatic arterial phase for detection–initial clinical experience, Radiology. 251 (2009) 771–779.

[10] B. Pregler, L.P. Beyer, A. Teufel, C. Niessen, C. Stroszczynski, H. Brodoefel, P. Wiggermann, Low Tube Voltage Liver MDCT with Sinogram-Affirmed Iterative Reconstructions for the Detection of Hepatocellular Carcinoma, Sci. Rep. 7 (2017) 9460.

[11] W.P. Shuman, D.E. Green, J.M. Busey, L.M. Mitsumori, E. Choi, K.M. Koprowicz, K. M. Kanal, Dual-energy liver CT: effect of monochromatic imaging on lesion detection, conspicuity, and contrast-to-noise ratio of hypervascular lesions on late arterial phase, AJR Am. J. Roentgenol. 203 (2014) 601–606.

[12] G.J. Hanson, G.J. Michalak, R. Childs, B. McCollough, A.N. Kurup, D.M. Hough, J. M. Frye, J.L. Fidler, S.K. Venkatesh, S. Leng, L. Yu, A.F. Halaweish, W.S. Harmsen, C.H. McCollough, J.G. Fletcher, Low kV versus dual-energy virtual monoenergetic CT imaging for proven liver lesions: what are the advantages and trade-offs in conspicuity and image quality? A pilot study, Abdom Radiol (NY). 43 (2018) 1404–1412.

[13] P. Lv, X.Z. Lin, K. Chen, J. Gao, Spectral CT in patients with small HCC: investigation of image quality and diagnostic accuracy, Eur. Radiol. 22 (2012) 2117–2124.

[14] S.-Y. Gao, X.-P. Zhang, Y. Cui, Y.-S. Sun, L. Tang, X.-T. Li, X.-Y. Zhang, J. Shan, Fused monochromatic imaging acquired by single source dual energy CT in hepatocellular carcinoma during arterial phase: an initial experience, Chin. J. Cancer Res. 26 (2014) 437–443.

[15] J. Yoo, J.M. Lee, J.H. Yoon, I. Joo, E.S. Lee, S.K. Jeon, S. Jang, Comparison of low kVp CT and dual-energy CT for the evaluation of hypervascular hepatocellular carcinoma, Abdom Radiol (NY). 46 (7) (2021) 3217–3226.

[16] M. Matsuda, T. Tsuda, T. Kido, H. Tanaka, H. Nishiyama, T. Itoh, K. Nakao, M. Hirooka, T. Mochizuki, Dual-Energy Computed Tomography in Patients With Small Hepatocellular Carcinoma: Utility of Noise-Reduced Monoenergetic Images for the Evaluation of Washout and Image Quality in the Equilibrium Phase, J. Comput. Assist. Tomogr. 42 (2018) 937–943.

[17] S. Yukisawa, H. Okugawa, Y. Masuya, S. Okabe, H. Fukuda, M. Yoshikawa, M. Ebara, H. Saisho, Multidetector helical CT plus superparamagnetic iron oxide-enhanced MR imaging for focal hepatic lesions in cirrhotic liver: A comparison with multi-phase CT during hepatic arteriography, Eur. J. Radiol. 61 (2007) 279–289.

[18] Y. Imai, T. Murakami, M. Hori, K. Fukuda, T. Kim, T. Marukawa, H. Abe, M. Kuwabara, H. Onishi, K. Tsuda, Y. Sawai, M. Kurokawa, N. Hayashi, M. Monden, H. Nakamura, Hypervascular hepatocellular carcinoma: Combined dynamic MDCT and SPIO-enhanced MRI versus combined CTHA and CTAP, Hepatol. Res. 38 (2008) 147–158.

[19] H.-J. Jang, J.H. Lim, S.J. Lee, C.K. Park, H.S. Park, Y.S. Do, Hepatocellular Carcinoma: Are Combined CT during Arterial Portography and CT Hepatic Arteriography in Addition to Triple-Phase Helical CT All Necessary for Preoperative Evaluation? Radiology. 215 (2000) 373–380.

[20] Y. Shinagawa, K. Sakamoto, K. Sato, E. Ito, H. Urakawa, K. Yoshimitsu, Usefulness of new subtraction algorithm in estimating degree of liver fibrosis by calculating extracellular volume fraction obtained from routine liver CT protocol equilibrium phase data: Preliminary experience, Eur. J. Radiol. 103 (2018) 99–104.
[21] H. Iizuka, Y. Yokota, M. Kidoh, S. Oda, O. Ikeda, Y. Tamura, Y. Funama, D. Sakabe, T. Nakaura, Y. Yamashita, D. Utsunomiya, Contrast Enhancement Boost Technique at Aortic Computed Tomography Angiography: Added Value for the Evaluation of Type II Endoleaks After Endovascular Aortic Aneurysm Repair, Acad. Radiol. 26 (2019) 1435–1440.
[22] W.D. Foley, T.A. Mallisee, M.D. Hohenwalter, C.R. Wilson, F.A. Quiroz, A.J. Taylor, Multiphase hepatic CT with a multirow detector CT scanner, AJR Am. J. Roentgenol. 175 (3) (2000) 679–685.
[23] T. Murakami, T. Kim, M. Takamura, M. Hori, S. Takahashi, M.P. Federle, K. Tsuda, K. Osuga, S. Kawata, H. Nakamura, M. Kudo, Hypervascular hepatocellular carcinoma: detection with double arterial phase multi-detector row helical CT, Radiology. 218 (2001) 763–767.
[24] S.H. Kim, A. Kamaya, J.K. Willmann, CT perfusion of the liver: principles and applications in oncology, Radiology. 272 (2014) 322–344.
[25] American College of Radiology. Liver Imaging Reporting and Data System. https://www.acr.org/Clinical-Resources/Reporting-and-Data-Systems/LIRADS. Accessed April 5, 2022.
[26] D.P. Chakraborty, Analysis of location specific observer performance data: validated extensions of the jackknife free-response (JAFROC) method, Acad. Radiol. 13 (2006) 1187–1193.
[27] D.P. Chakraborty, Validation and statistical power comparison of methods for analyzing free-response observer performance studies, Acad. Radiol. 15 (12) (2008) 1554–1566.